JACS
JOURNAL OF THE AMERICAN CHEMICAL SOCIETY
Article
pubs.acs.org/JACS

The Role of Reducible Oxide–Metal Cluster Charge Transfer in Catalytic Processes: New Insights on the Catalytic Mechanism of CO Oxidation on Au/TiO_2 from ab Initio Molecular Dynamics

Yang-Gang Wang,[†,‡] Yeohoon Yoon,[‡] Vassiliki-Alexandra Glezakou,[‡] Jun Li,*[,†,‡] and Roger Rousseau*[,‡]

[†]Department of Chemistry, Tsinghua University, Beijing, 100084, China

[‡]Institute for Interfacial Catalysis, Pacific Northwest National Laboratory, Richland, Washington 99352, United States

Supporting Information

ABSTRACT: To probe metal particle/reducible oxide interactions density functional theory based ab initio molecular dynamics studies were performed on a prototypical metal cluster (Au_{20}) supported on reducible oxides (rutile TiO_2(110)) to implicitly account for finite temperature effects and the role of excess surface charge in the metal oxide. It is found that the charge state of the Au particle is negative in a reducing chemical environment whereas in the presence of oxidizing species coadsorbed to the oxide surface the cluster obtained a net positive charge. In the context of the well-known CO oxidation reaction, charge transfer facilitates the plasticization of Au_{20}, which allows for a strong adsorbate induced surface reconstruction upon addition of CO leading to the formation of mobile Au–CO species on the surface. The charging/discharging of the cluster during the catalytic cycle of CO oxidation enhances and controls the amount of O_2 adsorbed at oxide/cluster interface and strongly influences the energetics of all redox steps in catalytic conversions. A detailed comparison of the current findings with previous studies is presented, and generalities about the role of surface–adsorbate charge transfer for metal cluster/reducible oxide interactions are discussed.

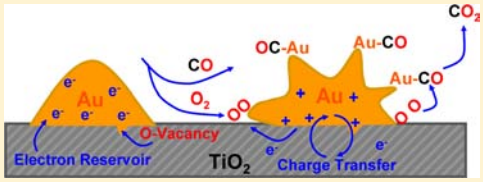

1. INTRODUCTION

The need for cleaner, cheaper, and renewable energy has become a major focus of the scientific and engineering communities. A critical component in this research is to advance our understanding of catalytic systems, which are vital to alternative energy sources as diverse as fuels from biomass conversion, chemical storage of energy, and creating carbon-neutral energy sources.[1] Theory and computation have played an important role in understanding and predicting chemical reactivity on metal surfaces and nanoparticles[2,3] by providing detailed mechanistic insights, interpretations of experimental phenomena, and even prediction of improved catalysts. Nonetheless, it is still very much a grand challenge to perform atomistic simulations of complex models of catalysts under realistic conditions including metal catalyst particles, reactants and products, support materials, and finite temperature.[4−11] Nowhere is this more true than for catalytic systems exhibiting strong metal–support interactions (SMSI).[12] Prototypical examples of this phenomena are observed for metal particles on reducible oxide supports, such as CeO_2 and TiO_2, where in addition to the above-mentioned complexities, one must also consider the origin, location, and transport of excess charge carriers across the metal/oxide interface throughout the entire catalytic process.[13−16]

The specific aim of the current study is to present results on ∼1 nm Au_{20} particles on partially reduced TiO_2 surface slab models in the context of the CO oxidation reaction to elucidate how finite temperature dynamics of metal particles and substrate/metal particle charge transfer contribute to the catalytic activity of TiO_2-supported Au nanoparticles. We have chosen this particular system for a variety of reasons: (i) Charge transport and its influence on reactivity has been relatively well studied in the context of TiO_2 surface chemistry.[17−28] Specifically, we have chosen the rutile TiO_2(110) surface with excess electrons resulting from the formation of oxygen vacancies (O_v) where extensive studies have already well characterized the nature of the charge carriers and their transport.[29−32] (ii) Gold nanoparticles, particularly Au_{20}, have also been well-characterized theoretically in previous studies with respect to their reactivity toward CO oxidation[33−47] and their well-known strongly anharmonic dynamical behavior at finite temperature.[48−52] (iii) Finally, there exist a wealth of experimental and theoretical studies using more traditional (at T = 0 K) potential energy surfaces to compare and contrast our findings and provide a measure of what new types of behavior one can expect by including these additional complexities into catalyst models.

We briefly review our current understanding of this chemistry. Gold has been widely used as a catalyst ever since nanosized gold particles supported on reducible oxides were found to be particularly effective for a variety of important catalytic reactions by Haruta, Hutchings, and others.[53−58] The role of the reducing nature of the support is largely attributed to charge donation to[59−63] or withdrawal from[64−70] gold or the possible charge build up at the metal/oxide interface or

Received: February 26, 2013
Published: June 19, 2013

   dx.doi.org/10.1021/ja402063v | J. Am. Chem. Soc. 2013, 135, 10673−10683

both.[71−74] Thus, implicit in our understanding of how reducible supports influence Au cluster chemistry in the context of the CO oxidation reaction is the potential to gain insights into many other similar processes catalyzed by metal clusters supported on reducible oxides. While reduced metal-oxide supports seem to be mandatory for gold nanoparticles to be catalytic,[75−77] later it was found that small size gold nanoparticles could also catalyze reactions even on inert supports.[78] Furthermore, subnanometer-sized gas-phase (or soft-landed) gold clusters are active as catalysts as well.[79−82]

The presence of the oxygen vacancy defects, which engender excess electron charge carriers at the surface of reducible oxides, is believed to play an important role in the catalytic oxidation by facilitating the O_2 activation or the electronic interaction with the Au cluster.[19,63,73,83−87] However, controversies still exist on the following issues: the interaction between supports and gold particles (binding sites, charge transfer, interfacial effect, etc.),[69,88−92] the charge state of supported Au nanoparticles (cationic, anionic or metallic) and its role in the reaction process,[17,52,93−99] and the active site of supported Au nanoparticles.[63,75,84,100−102] Nonetheless, nearly all theoretical studies on the Au/TiO_2 system were based on selected model clusters on surfaces where the presence of the itinerant excess electrons in the reducible support was not fully accounted for, nor were finite temperature effects included, despite the well-known tendency of Au nanoparticles and surface to exhibit large amplitude motions and disorder at finite temperatures.

In this work, we have investigated Au_{20} clusters supported on partially reduced rutile TiO_2(110) surface slab models by using ab initio molecular dynamics (AIMD) simulations, which allow for better sampling of possible surface sites and configurations. Our approach confirms some of the previously proposed mechanisms of CO oxidation on TiO_2 surfaces but provides new insights. It is found that calculated reaction energetics are highly sensitive to the charge state of the Au cluster for redox processes, and thus it is critical to evaluate the nature of the charge state of the surface under operando conditions. We show that the charge state of the gold nanoparticle is highly sensitive to the nature of the chemical environments, leading to significant cluster/support charge transfer across the adsorbate/oxide interface. More specifically, Au is negatively charged under reducing conditions and positively charged under oxidizing conditions. The Au clusters act as a reservoir of charge throughout the catalytic cycle facilitating both reduction processes involving the O_2 molecule and oxidation processes, such as the transformation of CO to CO_2. At finite temperatures, the stable high-symmetry Au_{20} cluster becomes liquid-like (i.e., plastic) upon charge transfer to or from the surface. Subsequently, large adsorbate-induced reconstruction takes place allowing for facile transfer of adsorbed CO to the metal/oxide interface, where the CO_2 formation reaction occurs.

2. COMPUTATIONAL DETAILS

The calculations were carried out using density functional theory (DFT) with the spin-polarized gradient corrected functional of Perdew, Burke, and Ernzerhof (PBE) as implemented in the CP2K package.[103−105] The wave functions were expanded in a molecularly optimized double-ζ Gaussian basis set to minimize basis set superposition errors.[106] An additional auxiliary plane wave[107] basis of 350 Ry energy cutoff was used for the calculation of the electrostatic energy terms. Core electrons have been modeled by scalar relativistic norm-conserving pseudopotentials[108,109] with 4, 6, 11, and 12 valence electrons of C, O, Ti, and Au, respectively. The Γ-point approximation was employed for Brillouin Zone integration. To understand the charge interaction between Au cluster and TiO_2 support, the accurate description of redox properties of reduced TiO_{2-x} substrate is necessary. Thus DFT+U theory[110] is used with U = 13.6 eV applied to the Ti 3d electrons within a local spin density approximation. This value of U adopted was found to adequately reproduce the experimental band gap, 3.0 eV, work function, W = 5.1 eV,[111] and location of defect states at ∼1.20 eV below conduction band.[29,112] We point out that the large U value may affect the estimation of the energy difference for the process involving the direct transfer of excess 3d electrons such as the binding energy of the Au cluster or O_2 on a reduced TiO_{2-x} support, but it will have only secondary affects on the processes occurring on Au_{20}/TiO_{2-x} because no excess charges are found to be localized on Ti 3d states. Further discussion and details are included in the Supporting Information where the U dependence of all the main conclusions of this study are examined and discussed.

A rutile TiO_2(110)-$p(6 \times 3)$ surface slab model was used to model the TiO_2 substrate. The slab consists of four O−Ti−O trilayers (12 atomic layers) with the bottom two O−Ti−O layers kept frozen, while the remaining layers were allowed to relax. All the slabs were repeated periodically with a 20 Å vacuum layer between the images in the direction of the surface normal. Detailed discussion of the reactivity and binding energy and their dependence on TiO_2 slab thickness can be found elsewhere,[28,113] and in general the current approach provides energetics converged within 0.2 eV with respect to thicker slabs. For convenience, the TiO_2 substrate with one bridged oxygen vacancy is denoted as TiO_{2-x} throughout the document.

A tetrahedral Au_{20} cluster was chosen to model Au nanoclusters, because it is a structurally well characterized stable gold particle.[33,34,36,38,39] Due to its closed electronic shell and tetrahedral symmetry, it is known to be relatively inert.[35,114] We benchmarked our current approach with respect to a family of Au_{20} isomers and found the current results reproduced structural parameters and relative energetics in accord with results from the literature; see Supporting Information. This idealized cluster serves as an extreme case of a gold cluster that is *least* likely to react with CO and O_2 or to have strong dynamic fluctuations. The schematic diagrams of the reduced TiO_2(110) surface, the tetrahedral Au_{20} cluster, and the relevant nomenclature of the various atomic sites described in this work are shown in Figure 1.

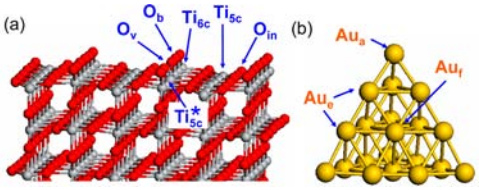

Figure 1. Schematic diagrams of the reduced TiO_2(110) surface (a) and the tetrahedral Au_{20} cluster (b). The surface layer of TiO_2 contains bridged oxygen atoms (O_b), in-plane oxygen atoms (O_{in}), 5-fold-coordinated Ti atoms (Ti_{5c}) and 6-fold-coordinated Ti atoms (Ti_{6c}). The oxygen vacancy is denoted as O_v. The two 5-fold-coordinated Ti atoms at the oxygen vacancy site are specially denoted as Ti^*_{5c}. The tetrahedral Au_{20} contains 4 apex Au atoms (Au_a), 12 edge Au atoms (Au_e), and 4 face-center Au atoms (Au_f).

All molecular dynamics simulations are performed by sampling the canonical (NVT) ensemble employing Nose−Hoover thermostats[115,116] with a time step of 0.5 fs during more than 30 ps of well-equilibrated trajectory. The relatively short time scales of AIMD limit sampling to only very fast, low-energy barrier events and preclude the observation slow processes. To partially overcome this limitation, we have performed simulations at both high temperatures (to more rapidly explore a large volume of phase space) and low ones (to sample fluctuations relevant to low temperature reactivity). To access the impact of surface/cluster charge transfer on cluster structure and facilitate statistical sampling, a temperature of 700 K, where the high

dx.doi.org/10.1021/ja402063v | J. Am. Chem. Soc. 2013, 135, 10673−10683

temperature CO oxidation reaction can occur, was chosen, though reactivity was simulated at more mild conditions of 120 K to find the low-energy reaction paths. The calculation of all reaction paths was performed using the climbing image nudged-elastic-band method (CI-NEB)[117,118] including seven replicas. Minimization of our CI-NEB was performed by ab initio molecular dynamics where each replica of the NEB is given an initial temperature of 300 K and annealed to 0 K over a time scale of 1−2 ps leading to a residual maximum component to the forces on the atoms of less than 1×10^{-3} atomic units. This approach allows us to explore the nearby configurations in phase space to obtain a path that may be substantially different, and lower in energy, than our initial conditions but does not guarantee that we have the absolute lowest energy path connecting two intermediates.

The electrostatic (Hartree) potential, V_H, is defined as the electrostatic energy an electron experiences from all the nuclei and other electrons in the system and provides a *quantitative* measure of the system work function and interfacial dipole layer. Here, V_H is used as a measure of the interfacial electrostatics and the cluster/support charge transfer between the Au nanocluster and TiO_2, as shown in previous studies by our group for both Au surfaces and TiO_2.[119,120] The charge transfer potential is calculated by considering the difference between V_H of the total system and the sum of the potentials obtained from the isolated neutral surface slab and Au_{20} cluster at fixed geometries. The direction of charge transfer can be identified from this quantity: increasing for charge transfer from the substrate to the adsorbate and decreasing for the converse process (see Figure 2). The net charge transfer, δq can be estimated assuming a

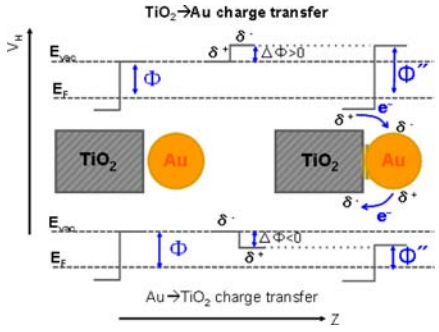

Figure 2. Schematic representation of the relationship between Hartree potential (V_H) and charge transfer. The shape of V_H at the crystal boundary is schematized as a step function for simplicity.

plate-capacitor model, $\delta q = \Delta V_H/(4\pi\rho d)$ where ΔV_H is defined as the change in V_H due to the induced surface dipole potential, ρ is the dipole moment density, and d is the separation distance.[119,121] This allows us to *unambiguously* identify charge transfer by directly accessing the electrostatic terms within the Hamiltonian, circumventing the prejudices of various population analysis methods. This approach is used here to calibrate the traditional Bader charge analysis on the simplest system such that it can be used with confidence in the more complex case where we consider the metal cluster, support, and a high coverage of reactants.

3. RESULTS AND DISCUSSION

3.1. The Adsorption of Au_{20} on a TiO_2 Support. The interaction between gold and the supported oxide plays a crucial role in the geometric and electronic properties of gold cluster and strongly affects the catalytic activity, thus it is important to first understand the structural behavior of Au particles on the oxide outside the context of the catalytic process. It is also important to understand the nature and magnitude of support/cluster charge transfer and how this is influenced by the presence of reactant and product molecules.

We first consider the result of AIMD simulations at 700 K for the isolated Au_{20} cluster and the Au_{20}/TiO_2 and Au_{20}/TiO_{2-x} systems used to illustrate the influence of finite temperature dynamics on the isolated gold cluster, by both a stoichiometric and a reduced TiO_2 substrate, respectively. The final configurations from our AIMD simulations are shown in Figure 3a−c. To demonstrate the differences between these

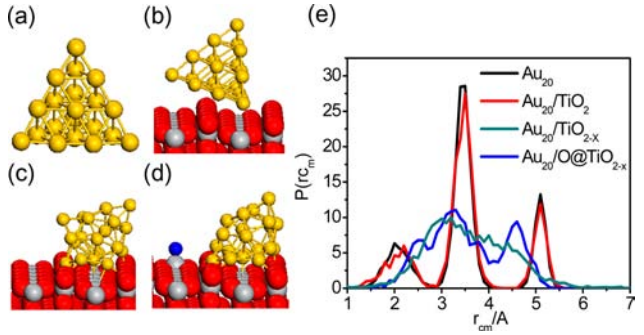

Figure 3. The final configurations from ~30 ps MD simulations at 700 K: (a) isolated Au_{20} cluster; (b) stoichiometric $TiO_2(110)$ supported Au_{20} cluster; (c) reduced $TiO_2(110)$ supported Au_{20} cluster after removal of a bridged oxygen atom; (d) reduced $TiO_2(110)$ supported Au_{20} cluster with one extra oxygen atom (blue atom) adsorbed at Ti_{5c} site. (e) Corresponding probability distribution functions $P(r_{cm})$ of the Au atoms relative to the center of mass of the Au_{20}.

systems, the distribution, $P(r_{cm})$, of the distance of Au atoms relative to the center of mass of the Au_{20} cluster is also shown in Figure 3e; additional quantities obtained from AIMD simulations are available in the Supporting Information. Due to its high stability, the isolated Au_{20} cluster retains its tetrahedral configuration even at the simulation temperature of 700 K, in accordance with previous work that shows that the structure does not isomerize below 800 K.[50] To quantify the rigidity or plasticity of the cluster, we consider the quantity, δ, based on the root mean squared bond length fluctuations:

$$\delta = \frac{2}{n(n-1)} \sum_{i<j} \frac{\sqrt{\langle r_{ij}^2 \rangle - \langle r_{ij} \rangle^2}}{\langle r_{ij} \rangle}$$

Based on a Linedman type criterion,[122] a value of $\delta \approx 5\%$ would indicate that at 700 K, the Au_{20} cluster is below its melting temperature; signified by a value of $\delta = 10\%$ or larger. As a result, the $P(r_{cm})$ of an isolated Au_{20} exhibits three well-defined peaks clearly separated by zero probability density between them. The peaks with maxima at 1.9, 3.3, and 4.9 Å correspond to the 4 face-centered Au atoms, the 12 edge Au atoms, and the 4 apex Au atoms, respectively. Similarly, the supported Au_{20} on the stoichiometric TiO_2 surface, exhibits a distribution probability, $P(r_{cm})$, almost identical to that of the gas phase cluster, Figure 3b,e, with $\delta = 6\%$. From the corresponding trajectory, the cluster can be seen to move freely along the row of Ti_{5c} atoms, while maintaining a T_d-like configuration. Furthermore, as shown in Figures S6 and S7 in Supporting Information, the pair distribution functions $g(r_{Au\text{-}O_b})$ and $g(r_{Au-Ti_{5c}})$ do not display well-resolved peaks that would be indicative of strong $Au-Ti_{5c}$ or $Au-O_b$ bonding.

On defected TiO_2 surface however, oxygen vacancies cause dramatic changes to the supported Au_{20} clusters, primarily by strongly binding through one of the apical Au atoms. In accord with this observation, experiments by Tong et al. found that Au^+ fills the vacancy hole on $TiO_2(110)$ surface with O-

dx.doi.org/10.1021/ja402063v | J. Am. Chem. Soc. 2013, 135, 10673−10683

defects.[123] In addition to the strongly bound Au atom, other parts of the cluster become involved in bonding interactions with Ti ions along the Ti_{5c} row. The pair distribution function $g(r_{Au-Ti_{5c}})$ (see Figure S6, Supporting Information) also shows direct evidence of a Au−Ti bond with a distinct peak around 2.8 Å. The average total number of Au−Ti_{5c} bonding interactions is ∼5.5, which includes both bonds with Ti_{5c} atoms and Ti at the oxygen defect site. While this observation is in accord with Metiu and co-worker's recent findings that show that the presence of the oxygen vacancy activates the Ti_{5c} atoms and leads to interaction with Au cluster,[90,91] it is in direct contrast to Hammer and co-worker's finding that Au atoms on top of such vacancy sites prefer to bind mainly to O_b rows rather than reach down to the substrate Ti atoms.[85] It is noted, however, that the former studies are performed on reduced TiO_2 models while the latter are models of oxidized TiO_2; see below for further discussion. Finally, compared with the stoichiometric support, the cluster on the defected-support exhibits a probability function $P(r_{cm})$ with significantly broader peaks and nonzero density between them, indicating that the cluster has become significantly more plastic. Not surprisingly, the estimated value of δ = 26% implies that the Au_{20} cluster is essentially melted, consistent with previous observations of liquid-like properties of supported Au cluster.[55,124] Note that although it has been suggested that at temperatures as high as 700 K SMSI may lead to Au clusters wetting the TiO_2 surface,[125,126] this tendency is not observed in present study.

Let us now consider the question of the charge state of the adsorbed Au_{20} cluster. The binding energy, E_b, is estimated to be ∼4.6 eV on the reduced TiO_2−O_V surface, which is significantly larger than the binding energy on the stoichiometric surface, ∼1.2 eV. The large E_b for the reduced oxide implies significant substrate-to-cluster charge transfer in the reduced surface case. To understand the electronic nature of the interaction process between Au cluster and TiO_2 surface, we consider the Hartree potential, V_H, see Figure 4,. The charge

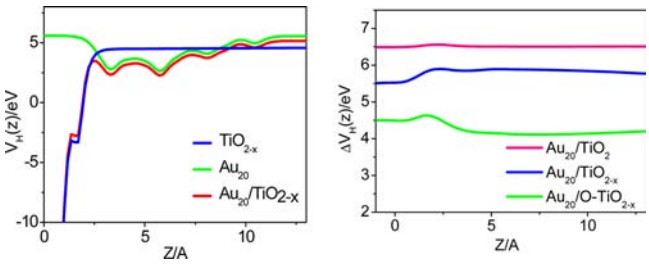

Figure 4. The Z projection of V_H for Au_{20}/TiO_{2-x} (a) and the charge transfer potentials for Au_{20}/TiO_2, Au_{20}/TiO_{2-x}, $Au_{20}/O-TiO_{2-x}$ (b). Note potentials in panel b are shifted by arbitrary values.

transfer potential for Au_{20}/TiO_2 is practically a constant with little fluctuation at the interface area compared with the step-like potential when a surface defect is present. This indicates that no appreciable charge transfer takes place between the Au_{20} cluster and the stoichiometric TiO_2 surface.

For the Au_{20} supported by TiO_{2-x}, the dipole potential shows a shift down by ∼0.37 eV, indicating that Au_{20} cluster is reduced by the surface and becomes negatively charged. The estimated charge of Au_{20} based on the plate-capacitor model is $-0.41e^-$, while the Bader charge analysis of Au_{20} is estimated to be $-1.02e^-$. Previous XPS data for clusters on surfaces under UHV conditions have also provided direct evidence that a reduced TiO_2(110) surface can transfer electrons to adsorbed Au clusters.[127]

It is noted that charge transfer is also expected to occur for O_2 molecules that are present in the CO oxidation reaction. These are expected to be significantly stronger oxidizers than any gold cluster.[21,128] To understand the implications of this observation we examine a hypothetical model where an oxygen adatom, O_v (a species postulated to exist during catalysis), is added to the TiO_{2-x} substrate. This can effectively remove the $2e^-$ the two excess electrons created by the oxygen vacancy and create an O^{2-} surface-bound adatom as seen in STM experiments.[21,128,129] Although the TiO_2 substrate has no excess electrons, it still differs from the case of stoichiometric TiO_2 in that the presence of excess negative charge at the surface is expected to raise the work function of the oxide making the surface more likely to be oxidizing. For this model, it is found that the TiO_2 surface effectively oxidizes the Au_{20} cluster resulting in a metal to substrate charge transfer estimated by a plate-capacitor model to be +0.19 e^- and Bader population analysis of around +0.08 e^-. Moreover, the Au−TiO_2 surface bonding changes significantly in that there is an increase in the total number of direct Au−O bonds to about 5, see Figure S7, Supporting Information. This model shows that there exist serious implications for the charge state of Au_{20} on the surface under an oxidizing environment that can in turn have appreciable influence on the nature or types of sites present under reactive conditions. The estimated δ value for this system is ∼15%, implying that the oxidized Au_{20} cluster is also melted at 700 K. Similarly, Metiu and co-workers also reported that the adsorption of O_2 on the oxide changes the structure of a Au_4 cluster adsorbed on the surface.[130]

Ultimately, this variation of the charge state of the Au_{20} cluster can be traced back to the similarity in the electronic chemical potential (the work function) of the cluster and the TiO_2(110) surface. As noted in section 2, for our DFT+U scheme, we have chosen a U value such that it reproduces the work function of a partially reduced TiO_2. This value was set to 5.1 eV, very similar to the value of the electronic chemical potential of 5.0 eV calculated for the Au_{20} cluster. Thus, the Au_{20} cluster and the substrate are well matched in terms of electronic chemical potential. This implies that charge may flow relatively easily between the cluster and support and can be strongly influenced by the presence of additional chemical species at the surface.

3.2. Co-adsorption of O_2 and Au_{20}. Given the above observation, it is necessary to delve deeper into the nature of the surface/adsorbate charge transfer when both Au_{20} and O_2 molecules are coadsorbed. We note, however, that the amount of charge available at the rutile TiO_2(110) surface with an O_v defect is still a matter of debate. Although, O_v defects, in principle, release $2e^-$ into the lattice (also accounted for in the above model), it has also been proposed that as many as $4e^-$ may be available from Ti^{3+} interstitial sites located within the bulk.[21,25,62,129,131] A detailed discussion of this point is beyond the scope of the current study, and here we will limit ourselves to considering the case where there are only two excess electrons available at the surface, though we do consider the case of higher reduction levels in data included in the Supporting Information. In addition, it has been noted by several studies[18,132,133] that these excess charge carriers are highly mobile within the bulk and are considered to be able to move freely to the surface where they reduce strongly oxidizing adsorbates such as O_2. Below we will examine this scenario,

although we stress that the following arguments are purely thermodynamic in nature and do not factor in the potential kinetic complexities, which might arise during surface/adsorbate charge transfer.

O_2 is known to bind to rutile TiO_2(110) preferentially at an O_v site.[21,134] In the current surface slab model, O_2 has a binding energy E_b = −5.05 eV and exhibits an O−O bond of 1.49 Å (indicative of an O−O single bond) with a net Bader charge transfer of 1.35 e^-, effectively resulting in an adsorbed O_2^{2-} species. Further addition of O_2 leads to weakly bound ($E_b \approx 0.1$ eV) physisorbed molecules. No further charge transfer is observed, because all available excess electrons are scavenged by the first O_2, in accord with previous calculations.[134] Further discussion of other charge states and binding configurations of O_2 on the surface can be found in our previous review.[21]

We now examine the case of O_2 adsorption on the Au_{20}/TiO_2 model presented above with the binding energies, bond lengths, and charge transfer data summarized in Table 1. We

Table 1. O_2 Adsorption Energies and Bader Charge of Au_{20} on TiO_{2-x}, Au_{20}/TiO_{2-x}[a]

		0 O_2	1 O_2	2 O_2	3O_2
TiO_{2-x}	E		−5.05	−0.11	−0.11
	L		1.49	1.49, 1.23	1.49, 1.23, 1.23
	Q		−1.35	−1.34, −0.01	−1.34, −0.00, −0.00
Au_{20}/TiO_{2-x}	E		−1.73	−0.83	−0.30
	L		1.49	1.49, 1.44	1.40, 1.44, 1.35
	Q		−1.24	−1.24, −0.98	−0.92, −1.01, −0.73
	Au_{20}	−1.02	+0.08	+0.90	+1.17

[a] E, binding energy (eV); L, O−O bond length (Å); Q, charge attained by O_2 (e^-). To better understand the charge state of Au_{20} upon O_2 adsorption, we also consider the extra excess electrons from surface hydroxyl and interstitial Ti (See Supporting Information).

begin with the simple case of considering O_2 adsorption solely on the exposed TiO_2 surface. Similar to the pristine surface, adsorption of a single O_2 molecule at a Ti_{5c} site leads to the formation of a chemisorbed O_2^{2-} species. In this process, the Au_{20} cluster shifts from a net negative charge of −1.24 e^- (as quantified by Bader population analysis) to a net neutral species, indicating that it has donated electrons to O_2 via the intervening substrate, even though it is not directly bound to the Au_{20} cluster (See Figure 5). In this vein, a second and to a

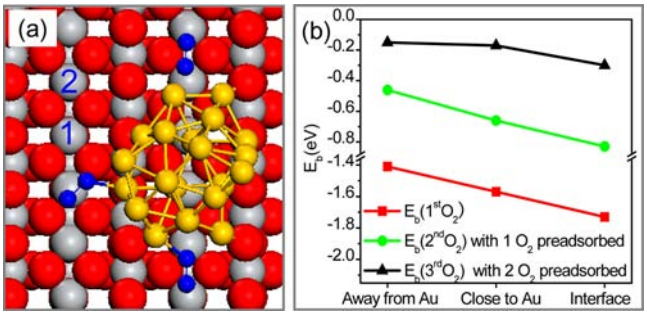

Figure 5. O_2 adsorption on Au_{20}/TiO_2. (a) The most stable adsorption configuration with three O_2 molecules adsorbed at the Au/TiO_2 interface. The other possible binding sites are also denoted as "1" (close to Au) and "2" (away from Au). (b) The adsorption energies for O_2 adsorbed at different binding sites.

lesser extent a third O_2 molecule can also be adsorbed at a Ti_{5c} site without being in direct contact with the Au_{20}. We note that the second O_2 exhibits a binding energy E_b = −0.83 eV with a bond length 1.44 Å indicating an O_2^{2-} state, whereas the third is more weakly bound with E_b = −0.30 eV, a charge transfer of only 0.27 e^-, and a bond length of 1.35 Å, consistent with an adsorbed O_2^- species. These additional O_2 species result in the oxidation of the Au_{20} cluster increasing its charge up to +1.17 e^-. Further addition of O_2 species does not lead to further chemisorption nor further oxidation of the Au_{20} cluster.

These results illustrate a critical principle. Like the surface without Au_{20}, the ability to adsorb oxygen is attenuated on the Au_{20}/TiO_2 surface by the ability to reduce the adsorbates. The fundamental difference is that the presence of the Au_{20} cluster enhances the charge available at the surface for O_2 reduction and thus effectively increases the amount of O_2 that can be adsorbed to the surface. As discussed in the Supporting Information, this trend is also preserved in the hypothetical case where there is more than $2e^-/O_v$ available at the surface to facilitate reduction.

So far we have demonstrated how surface-mediated charge transfer can be operative in these systems. As can be seen from Figure 6, the positive charge arising from the oxidation of the

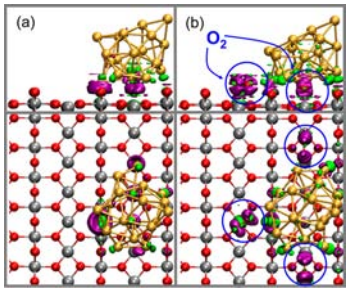

Figure 6. The electron density difference $\delta\rho$. (a) Au_{20}/TiO_{2-x}(110) without O_2 adsorption, $\delta\rho = \rho_{tot} - \rho_{Au_{20}} - \rho_{TiO_{2-x}}$. (b) Au_{20}/TiO_{2-x}(110) with three O_2 adsorbed at the interface, $\delta\rho = \rho_{tot} - \rho_{Au_{20}} - \rho_{TiO_{2-x}} - 3\rho_{O_2}$. The purple surface indicates the increase of electron density, and the green surface indicates the decrease of electron density.

Au_{20} cluster is preferentially located at the oxide/metal interface. As a result, chemisorbed (and negatively charged) O_2 species will preferentially reside at this interface as noted by several previous studies.[68,100,101] Nonetheless, the higher surface area of bare oxide implies that some O_2 species may reside on the oxide surface in an effective metastable preadsorbed state. Thus we compared the adsorption energies for O_2 adsorbed at different sites in Figure 5b, where it can be seen that as one transforms molecules from preadsorbed configurations to interfacial configurations, there is an additional gain in energy on the order of 0.1−0.3 eV. Thus it could be concluded that Au cluster acts as a reservoir and the O_2 molecules prefer to be activated at the interface.

3.3. CO Adsorption and Diffusion. In this subsection, we examine CO adsorption in the light of our observations of the dynamic plasticity of the Au_{20} particle, and the substrate/cluster charge transfer. Previous studies on Au clusters have also shown that they are indeed rather flexible in geometry and easily expose low-coordinated sites (such as 4-fold or lower) for binding CO molecules.[46,135−139] To address this issue, we performed AIMD simulation for CO adsorption on Au_{20}

dx.doi.org/10.1021/ja402063v | J. Am. Chem. Soc. 2013, 135, 10673−10683

supported by TiO_2 substrate at 700 K. Two O_2 molecules are allowed to preadsorb at the interface, and the third O_2 molecule with a physisorption binding energy 0.30 eV is neglected for further consideration, because it would be expected to desorb even at relatively low temperatures. The statistical configuration information of Au_{20} is shown in Figure 7.

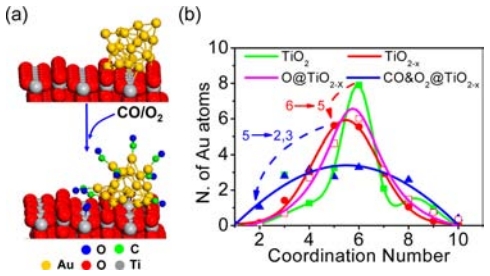

Figure 7. The morphology of Au cluster changes upon CO adsorption (a) and the statistical distribution curve of low coordinated Au atoms for Au_{20}/TiO_2, Au_{20}/TiO_{2-x}, and $CO@Au_{20}/TiO_{2-x}$ (b).

For isolated Au_{20}, it is known that Au_{20} has 4 apex Au atoms with coordination number CN = 8, 12 edge Au atoms with CN = 6, and the 4 face-center Au atoms with CN = 9. Because Au_{20} keeps the tetrahedral configuration on stoichiometric TiO_2 substrate, the number of low coordination sites is very close to four, corresponding to the four apex Au atoms. Though Au_{20} has four low-coordinated sites for binding, the larger Au clusters often used for catalysis exhibit a far lower percentage of these sites. When the Au cluster is supported by reduced or oxidized TiO_2 surface, the average number of low coordinated Au atoms does not distinctly change with 4.5 for reduced TiO_2 and 3.5 for oxidized TiO_2. The slightly low number for oxidized TiO_2 can be attributed to the formation of Au−O bonds, as is discussed in section 3.1. When the difference of the CN distributions is compared, defects tend to make the distributions broader, leading to an increase of 5-coordinated Au atoms. Thus one might conclude that there should be little effect on the ability to adsorb CO between the isolated cluster and the species present under strongly oxidizing conditions.

This turns out not to be the case. We consider the case where eight CO molecules are adsorbed on a Au_{20} cluster with two oxygen molecules that are allowed to coadsorb at the cluster/oxide interface as discussed above. The AIMD simulation shows that Au_{20} extrudes low-coordinated sites to bind CO. The statistical number of low-coordinated Au atoms is found to significantly increase with CO adsorption implying a strong *adsorption-induced surface reconstruction* similar in spirit to that previously reported for CO on small gas phase Au clusters.[46,135,136] Considering the binding energies (shown in Figure S8, Supporting Information), the system is estimated to be able to bind up to 10 CO molecules including 2 physisorbed CO molecules, far exceeding the 4 estimated by counting the low coordination sites on the bare clusters. The average binding energy per CO is estimated to be 0.94 eV. In addition, the charge of surface bound Au_{20} in the presence of 2 O_2 and 10 CO molecules is estimated to be +0.80 e^-, which is only 0.10 e^- lower than that with 2 O_2 molecules without any adsorbed CO, implying that CO has negligible impact on the charge state of the cluster. Comparably the isolated Au_{20} with 4 CO adsorbed at the apex site has a small net negative charge of $-0.14e^-$ and E_b = −1.03 eV per CO.

Since O_2 species preferentially reside at the gold−oxide interface, CO mobility toward the interface is vital for CO oxidation. True to the point, our AIMD simulations reveal a unique feature of this system, exposed in select snapshots of the MD trajectory in Figure 8a. It was found that CO is not able to

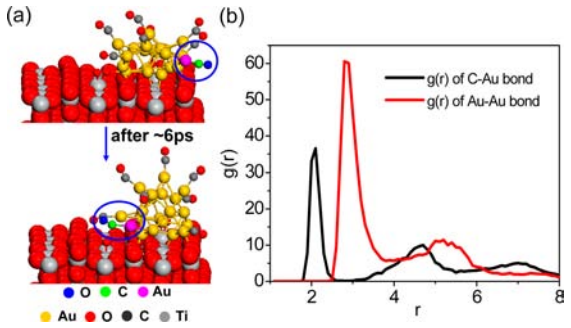

Figure 8. (a) Selected snapshots of the MD trajectory for Au_{20}/TiO_{2-x} to show the diffusion of the OC−Au part. (b) The radio bond distributions for Au−C and Au−Au bonds.

diffuse freely from one Au site to another Au site; it can however move easily to the interface by carrying along the Au atom to which it is bound. To provide a more quantitative description of this phenomenon, we compare the radial distribution functions of Au−C and Au−Au contacts, shown in Figure 8b. In $g_{Au-C}(r)$, there is a zero density regime between the first two peaks, indicating that once a strong Au−C bond is formed, it does not break on the time scale of our simulation. This result is consistent with previous vibrational spectroscopy observation of highly stable Au−CO complexes in the gas phase.[60] In contrast, the $g_{Au-Au}(r)$ is broad with appreciable density between the main peaks, which is indicative of the more liquid-like state of the Au particles. Therefore, the operative species for molecular transport is in fact a Au−CO unit that is indeed not realized by previous studies. As a prominent example, the recent study by Green and co-workers[100] inferred that CO adsorbed at the sites on the Au cluster was inactive because it could not approach the activated O_2 species at the interface according to the high calculated barrier of CO diffusion between two adjacent Au sites. Their discussion on CO transportation is problematic because the CO transport process is not done by the diffusion of CO itself but the whole Au−CO unit.

We note that experimental studies have already demonstrated CO oxidation catalyzed by TiO_2-supported Au nanoparticles within a large temperature range from 120 to 700 K[53,83,100,140,141] Thus, to explore the existence and transport of Au−CO species across the entire temperature range, an AIMD simulation at 120 K was performed, and a similar picture is observed (See Figure S9, Supporting Information). This result indicates that the liquid-like properties of Au_{20} can even take place in operando conditions at very low temperature. It is noted that at 700 K, the MD simulation indeed sees enhanced morphology changes of the Au cluster and transport of adsorbed CO (see Figure S10, Supporting Information). These observations are in accord with previous findings[141] that at a high-temperature TiO_2-supported Au nanoparticles became much more active for CO oxidation than at low temperature.

We also note that strong adsorbate induced surface reconstructions have been suggested to be linked to catalyst

dx.doi.org/10.1021/ja402063v | J. Am. Chem. Soc. 2013, 135, 10673−10683

degradation under operando conditions.[142−144] Recently, the disruption of a small Au cluster (Au_3) on the MgO surface has been reported from static DFT calculations.[145] Yet in the present study, it is observed that the Au_{20} cluster on reduced TiO_2 substrate remains intact during all MD simulations (~10 ps) even at 700 K, suggesting that the Au cluster would be at least metastable on the TiO_2 surface once it is anchored by the oxygen defect. We point out however that sintering of freely moving Au clusters at nondefect sites is highly likely.

In conclusion, the emerging picture is that charge transfer that helps induce plasticity into the Au cluster also has an influence on transport of species on the particle. As a result, the supported Au cluster is a very flexible and adaptable catalyst that both extrudes low-coordinated Au atoms to bind CO and allows for facile transport of these species to the interface where the activated O_2 species exist.

3.4. The Catalytic Cycle of CO Oxidation. We now consider the role of metal particle plasticity and charge transfer in the context of the catalytic cycle of CO oxidation. As noted in several theoretical calculations[79−82,102,146] for Au nanoclusters, the CO can react with O_2 molecules at the low-coordinated Au sites or step sites even without the need for a support. However, for Au_{20} supported on the TiO_2 surface, after considering a large number of different configurations of adsorbed O_2 with or without coadsorbed CO, we found that O_2 *does not* adsorb on the Au cluster. We also performed a short AIMD simulation with seven O_2 molecules initially close to different sites of the Au cluster at 120 K and found that after ~10 ps no O_2 is observed on the Au cluster (See Figure S11, Supporting Information). This suggests that direct oxidation of CO on the cluster is not an operative channel for this system, in accord with the experimental studies[83,100,147−149] showing that the metal/oxide interface is the preferred reaction site.

To probe the reactivity in an unbiased manner, we performed an AIMD simulation wherein we start our trajectory with two chemisorbed O_2 molecules at the Au_{20}/TiO_2 interface and six chemisorbed CO molecules on the Au cluster at 120 K. Individual snapshots from this trajectory of reactive events are shown in Figure 9. What we observe is that CO molecules

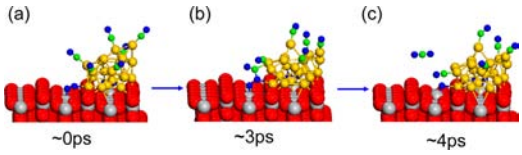

Figure 9. Snapshots for the reaction process $*CO + *O_2 \rightarrow CO_2 + *O$ at the Au_{20}/TiO_2 interface: (a) Initial configuration; (b) CO attachment to O_2 adsorbed at Au/oxide interface; (c) Desorption of CO_2.

quickly attach to the O_2 species bound at the interface. After only 4 ps, the CO reacts with the bound O_2 and releases a CO_2 molecule without rupturing the O−O bond *a priori*. This mechanism confirms previous findings[70,85,100,150] that CO oxidation occurs via a CO−O_2 intermediate at the interface and will form the basis of the further analysis presented in this section. Finally it is emphasized that we have not performed an exhaustive search for alternate reactive routes nor have we continued to propagate the trajectory to observe the removal of the second O atom left behind during the CO_2 formation step.

We further focus our discussion on the zero temperature potential energy, which allows us to compare our results with the large number of studies currently existing in the literature.[63,68,70,85,100,151,152] Figure 10 shows the lowest energy

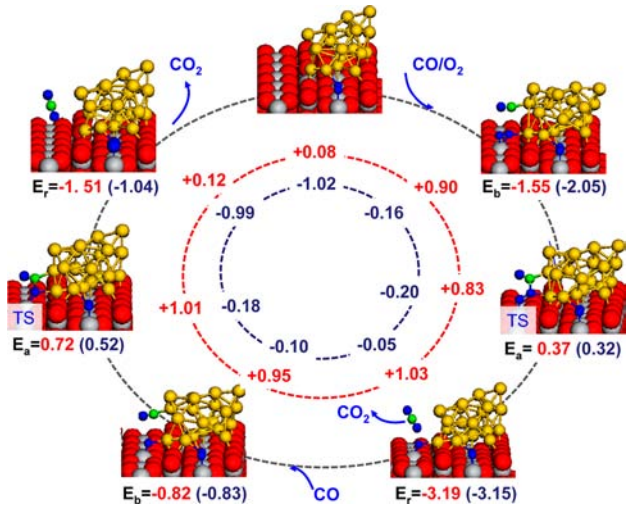

Figure 10. Catalytic cycle and corresponding charge cycle for CO oxidation at the interface of Au_{20} supported by reduced TiO_2 support. The energies are shown in the outer circle and the charges of the Au_{20} cluster are shown in the two inner circles. The red values correspond to Au/TiO_{2-x} system with two O_2 adsorbed (positively charged Au_{20}), while those in blue corresponds to that with only one O_2 adsorbed (negatively charged Au_{20}).

pathway for CO oxidation catalyzed by a positively charged Au cluster supported by a TiO_2 support, determined from our simulations. An alternate catalytic pathway can be found in the Supporting Information. For convenience of discussion, we tracked the Bader charges on the Au_{20} cluster throughout this process for each of the relevant stationary points on the potential energy surface. In this model, we included two adsorbed O_2 molecules to effectively scavenge all available charge at the surface as discussed in section 3.2, while only a single CO adsorbed to the cluster was considered for the sake of simplicity.

In the proposed mechanism, the O_2 molecule is first activated at the metal/oxide interface with a bond length of 1.44 Å consistent with a description of an adsorbed O_2^{2-} and a CO adsorbed onto the Au_{20} cluster. As discussed in section 3.3, this leaves the Au_{20} cluster partially oxidized with a charge of +0.9 *e*. Mobility of CO to the interface is facile where it can react with the bound O_2^{2-} with a low activation energy barrier of 0.37 eV to form an O^{2-} adatom bound to TiO_2 and a CO_2, which desorbs readily. Because the available charge at the surface remains on the surface-bound O^{2-}, there is no appreciable change in the charge state of Au_{20}, which remains oxidized. At this point, a second CO can also be adsorbed and transported to the metal/oxide interface to react with the O^{2-} species and complete the catalytic cycle. The activation energy of 0.72 eV for this step is larger than the first one, but it is still a relatively low barrier for processes even at ambient conditions. Most notably, it is at this stage that the Au_{20} cluster undergoes a change in its charge state to become significantly less (positively) charged. That is, Au_{20} is acting as a charge reservoir during the catalytic cycle and after the O^{2-} adatom is removed, the surface is able to further absorb additional O_2 species. Because both CO_2 formation steps are highly exothermic by at least 1.5 eV with relatively low activation

dx.doi.org/10.1021/ja402063v | J. Am. Chem. Soc. 2013, 135, 10673−10683

barriers, CO oxidation via this reaction channel is expected to be highly active.

In general, our results suggest that the Au cluster acts as a charge reservoir in the catalytic process. O_2 adsorption will scavenge all available surface charge in the oxygen-rich environment of a CO oxidation reaction. As discussed in sections 3.1 and 3.2, this would result in a positively charged Au species under operando catalysis conditions. Nonetheless reduced Au clusters can be generated transiently after release of CO_2 from the surface. However, the excess surface charge generated in this process can be readily scavenged by excess O_2 in the gas phase, and thus CO_2 production controls the rate of O_2 reductive chemisorption. Given the strong O_2 binding energy (see Supporting Information) additional doping of the TiO_2 to generate a large number of excess electrons at the surface may well lead to a larger coverage of surface-bound O_2 molecules (and thus enhance overall rates), but surface-bound O_2 would still only be replenished when a transient reduced Au-cluster species is produced.

The above discussion of the reaction cycle implies that the availability of charge at the surface can effectively control the amount of O_2 that is present for reaction with CO. To probe the influence of charge on the calculated energetics of the mechanism, we consider the same catalytic cycle with only a single O_2 molecule at the interface and thus have excess charge in the system. The barriers and reaction energies are also listed in the blue font in the outer circle in Figure 10, for comparison to the values of the catalytic cycle with two O_2 adsorbed. Not surprisingly, the first CO_2 formation event is essentially not influenced by this difference, because the Au_{20} cluster does not itself undergo a redox process. Remediakis et al also reported a similar barrier (~0.4 eV) on a Au cluster supported by an over-reduced TiO_2 support with three oxygen vacancies.[63] More specifically, the energetics for the first CO_2 production via $*CO + *O_2 \rightarrow *CO_2 + *O$ on the reduced TiO_2 supported Au cluster (negatively charged)[85] and an alkaline TiO_2 supported Au cluster (positively charged)[70] have been reported by Hammer and co-workers. Despite the different charge states of Au clusters in these models, the barriers and the reaction energies in these calculations are remarkably similar (~0.16 eV for barriers and approximately −3.0 eV for reaction energies). Thus, it can be concluded that the charge state of Au cluster has a negligible effect on the first CO_2 production because neither the surface nor the cluster undergoes a redox process.

This is not true for the second CO_2 formation step where the Au_{20} cluster undergoes a significant redox process with its charge state becoming less (positively) charged. For the scenario with a single O_2 at the interface where excess charge is not completely scavenged and Au_{20} is not fully oxidized, the activation energy for the second CO_2 formation is found to be appreciably lower by 0.2 eV and the overall reaction energy is about 0.5 eV less exothermic. From a kinetic perspective, this would imply that the first and second CO_2 production steps would be more similar in impact on the global rate of CO_2 production as opposed to the second being strongly rate determining when all excess surface charge is scavenged. Notably, our conclusion confirms recent experimental findings by Yates and his co-workers that CO oxidation on a preoxidized Au/TiO_2 catalyst is much less active than that on the reduced catalyst.[153] Similarly, Hammer and co-workers also reported a much smaller barrier (~0.01 eV) for the second CO_2 formation on an alkaline (strongly reduced) TiO_2 supported Au cluster, which also indicates that the highly reduced surface will be much more favorable for the second CO_2 formation. In addition, the charge state of Au cluster also significantly affects the binding energy of O_2 adsorption, as is discussed in section 3.2. According to the energetics of the catalysis, the total binding of the reactants (CO and O_2) will be ~0.5 eV less favorable when the surface is fully oxidized. Thus, we concluded that the charge state of Au cluster strongly influences the energetics of all redox steps in catalytic conversions.

Cooperative effects, arising at high CO coverage, might influence CO diffusion and potentially even the activation energy as has already been discussed on oxide-supported Au clusters in previous studies.[102,145] However, the adsorption of additional CO will not alter the relative comparison between different charge states of Au_{20} due to the negligible effect this has on the cluster charge state (see discussion in section 3.3). The emerging conclusion is that accurately accounting for the charge state of the cluster/support under operando catalytic conditions can have a profound impact on the quantitative information that can be extracted from simulation for steps that explicitly involve redox processes.

4. CONCLUSIONS

Our study has probed the influence of the charge state of reducible supports and its role in catalytic activity in unprecedented detail in the context of the CO oxidation for a model Au_{20}/rutile-TiO_2(110) interface. In the process, we have reconciled many (sometimes disparate) observations in the literature regarding the charge state of Au on these interfaces and reaction energetics.

In general terms, redox processes to or from the cluster are strongly dependent upon the chemical environment due largely to the matching in electronic chemical potentials between the cluster and the support. This allows charge to flow to or from the Au cluster depending on what species are adsorbed on the oxide support. Moreover, the charge state of the Au cluster has a strong influence on the structure and binding of the cluster to the surface, plasticity and fluidity of the cluster (and hence the ability to transport adsorbed molecules to and from reactive sites), and ultimately the reaction energetics for chemical steps that explicitly involve a change in redox state of the metal particle. These results have strong implications for our ability to properly model reactivity of these systems and point to the necessity of carefully quantifying and accounting for excess surface charge for these types of catalytic materials under reaction conditions.

Our study raises many additional fundamental questions. Although we believe that charge transfer will similarly influence reactivity for larger Au clusters, it is not clear at this point how much the cluster size may influence the amount of additional O_2 that can be adsorbed nor the degree to which the charge-induced cluster plasticity and adsorbate-induced metal surface reconstructions will be influenced. Generalization of these findings to a larger class of systems can be achieved by delineating the role of both redox processes and metal particle−oxide Lewis acid/base interactions as recently discussed by Metiu.[154] Our future work will consider how extensible the current findings are to other metal/reducible oxide systems, especially those where the electronic chemical potentials are not so well matched as for Au/TiO_2, including differences in support materials, reactive metals, and catalytic reactions, as well as the nature and type of charge- promoting defects in oxides.

■ ASSOCIATED CONTENT

Supporting Information

Test of property dependence on U value, energies of Au_{20} isomers, statistical quantities from Au_{20}/TiO_2 AIMD simulations, the effect of the extra excess electrons from surface hydroxyls and interstitial Ti atoms, CO coverage and binding energies, results of MD simulation for CO adsorption and diffusion at 120 K, an alternate catalytic pathway, and the absolute energies and the coordinates of the optimized molecules. This material is available free of charge via the Internet at http://pubs.acs.org.

■ AUTHOR INFORMATION

Corresponding Author

roger.rousseau@pnnl.gov; junli@tsinghua.edu.cn

Notes

The authors declare no competing financial interest.

■ ACKNOWLEDGMENTS

We thank Robert Weber, Zdenek Dohnalek, Nick Petrik, and Greg Kimmel for insightful discussions. Part of this work was supported by the U.S. Department of Energy, Office of Basic Energy Sciences, Division of Chemical Sciences, Geosciences & Biosciences, and performed at the Pacific Northwest National Laboratory (PNNL). PNNL is a multiprogram national laboratory operated for the DOE by Battelle. J. Li and Y.-G. Wang were also financially supported by NKBRSF (Grant 2011CB932400) and NSFC (Grant 91026003, 21101098) of China. Y.-G. Wang acknowledges the fellowship from China Scholarship Council and the PNNL-ASF fellowship program. Computational resources were provided at W. R. Wiley Environmental Molecular Science Laboratory (EMSL), a national scientific user facility sponsored by the Department of Energy's Office of Biological and Environmental Research located at PNNL and the National Energy Research Scientific Computing Center (NERSC) at Lawrence Berkeley National Laboratory.

■ REFERENCES

(1) Basic Research Needs: Catalysis for Energy. A.T. Bell, B. C. G., D.R. Ray, Report from the US Department of Energy Basic Energy Sciences Workshop, 2007. http://science.energy.gov/.

(2) Salciccioli, M.; Stamatakis, M.; Caratzoulas, S.; Vlachos, D. *Chem. Eng. Sci.* **2011**, *66*, 4319.

(3) Nørskov, J. K.; Bligaard, T.; Rossmeisl, J.; Christensen, C. H. *Nat. Chem.* **2009**, *1*, 37.

(4) Imbihl, R.; Behm, R. J.; Schlögl, R. *Phys. Chem. Chem. Phys.* **2007**, *9*, 3459.

(5) Campbell, C. T. *Nat. Chem.* **2012**, *4*, 597.

(6) Stakheev, A. Y.; Kustov, L. *Appl. Catal. A* **1999**, *188*, 3.

(7) Allian, A. D.; Takanabe, K.; Fujdala, K. L.; Hao, X.; Truex, T. J.; Cai, J.; Buda, C.; Neurock, M.; Iglesia, E. *J. Am. Chem. Soc.* **2011**, *133*, 4498.

(8) Lebarbier, V. M.; Mei, D.; Kim, D. H.; Andersen, A.; Male, J. L.; Holladay, J. E.; Rousseau, R.; Wang, Y. *J. Phys. Chem. C* **2011**, *115*, 17440.

(9) Ammal, S. C.; Heyden, A. *J. Chem. Phys.* **2010**, *133*, No. 164703.

(10) Vila, F.; Rehr, J.; Kas, J.; Nuzzo, R.; Frenkel, A. *Phys. Rev. B* **2008**, *78*, No. 121404.

(11) Kulkarni, A.; Lobo-Lapidus, R. J.; Gates, B. C. *Chem. Commun.* **2010**, *46*, 5997.

(12) Tauster, S. *Acc. Chem. Res.* **1987**, *20*, 389.

(13) Vayssilov, G. N.; Lykhach, Y.; Migani, A.; Staudt, T.; Petrova, G. P.; Tsud, N.; Skála, T.; Bruix, A.; Illas, F.; Prince, K. C. *Nat. Mater.* **2011**, *10*, 310.

(14) Zhang, C.; Michaelides, A.; Jenkins, S. J. *Phys. Chem. Chem. Phys.* **2010**, *13*, 22.

(15) Hegde, M.; Madras, G.; Patil, K. *Acc. Chem. Res.* **2009**, *42*, 704.

(16) Goodman, D. *Catal. Lett.* **2005**, *99*, 1.

(17) Camellone, M. F.; Kowalski, P. M.; Marx, D. *Phys. Rev. B* **2011**, *84*, No. 035413.

(18) Kowalski, P. M.; Camellone, M. F.; Nair, N. N.; Meyer, B.; Marx, D. *Phys. Rev. Lett.* **2010**, *105*, No. 146405.

(19) Wu, X.; Selloni, A.; Nayak, S. K. *J. Chem. Phys.* **2004**, *120*, 4512.

(20) Di Valentin, C.; Pacchioni, G.; Selloni, A. *Phys. Rev. Lett.* **2006**, *97*, No. 166803.

(21) Dohnálek, Z.; Lyubinetsky, I.; Rousseau, R. *Prog. Surf. Sci.* **2010**, *85*, 161.

(22) Liu, L.-M.; Crawford, P.; Hu, P. *Prog. Surf. Sci.* **2009**, *84*, 155.

(23) Du, Y.; Deskins, N. A.; Zhang, Z.; Dohnalek, Z.; Dupuis, M.; Lyubinetsky, I. *Phys. Chem. Chem. Phys.* **2010**, *12*, 6337.

(24) Wendt, S.; Bechstein, R.; Porsgaard, S.; Lira, E.; Hansen, J. Ø.; Huo, P.; Li, Z.; Hammer, B.; Besenbacher, F. *Phys. Rev. Lett.* **2010**, *104*, No. 259703.

(25) Wendt, S.; Sprunger, P. T.; Lira, E.; Madsen, G. K. H.; Li, Z.; Hansen, J. Ø.; Matthiesen, J.; Blekinge-Rasmussen, A.; Lægsgaard, E.; Hammer, B. *Science* **2008**, *320*, 1755.

(26) Bowker, M.; Bennett, R. A. *J. Phys.: Condens. Matter* **2009**, *21*, No. 474224.

(27) Pang, C. L.; Lindsay, R.; Thornton, G. *Chem. Soc. Rev.* **2008**, *37*, 2328.

(28) Chrétien, S.; Metiu, H. *J. Phys. Chem. C* **2011**, *115*, 4696.

(29) Yim, C.; Pang, C.; Thornton, G. *Phys. Rev. Lett.* **2010**, *104*, No. 036806.

(30) Krüger, P.; Jupille, J.; Bourgeois, S.; Domenichini, B.; Verdini, A.; Floreano, L.; Morgante, A. *Phys. Rev. Lett.* **2012**, *108*, No. 126803.

(31) Deskins, N. A.; Rousseau, R.; Dupuis, M. *J. Phys. Chem. C* **2011**, *115*, 7562.

(32) Liu, L.-M.; Crawford, P.; Hu, P. *Prog. Surf. Sci.* **2009**, *84*, 155.

(33) Li, J.; Li, X.; Zhai, H. J.; Wang, L. S. *Science* **2003**, *299*, 864.

(34) King, R. B.; Chen, Z.; von Ragué Schleyer, P. *Inorg. Chem.* **2004**, *43*, 4564.

(35) Heiz, U.; Sanchez, A.; Abbet, S.; Schneider, W. D. *Eur. Phys. J. D* **1999**, *9*, 35.

(36) Wang, J.; Wang, G.; Zhao, J. *Chem. Phys. Lett.* **2003**, *380*, 716.

(37) Ji, M.; Gu, X.; Li, X.; Gong, X.; Li, J.; Wang, L. S. *Angew. Chem., Int. Ed.* **2005**, *44*, 7119.

(38) Zhang, H. F.; Stender, M.; Zhang, R.; Wang, C.; Li, J.; Wang, L. S. *J. Phys. Chem. B* **2004**, *108*, 12259.

(39) Aikens, C. M.; Schatz, G. C. *J. Phys. Chem. A* **2006**, *110*, 13317.

(40) Zhai, H. J.; Kiran, B.; Dai, B.; Li, J.; Wang, L. S. *J. Am. Chem. Soc.* **2005**, *127*, 12098.

(41) Kryachko, E.; Remacle, F. *Int. J. Quantum Chem.* **2007**, *107*, 2922.

(42) Gruene, P.; Rayner, D. M.; Redlich, B.; van der Meer, A. F. G.; Lyon, J. T.; Meijer, G.; Fielicke, A. *Science* **2008**, *321*, 674.

(43) Zhu, M.; Qian, H.; Jin, R. *J. Am. Chem. Soc.* **2009**, *131*, 7220.

(44) Chang, C.-R.; Wang, Y.-G.; Li, J. *Nano Res.* **2011**, *4*, 131.

(45) Gao, Y.; Shao, N.; Pei, Y.; Chen, Z.; Zeng, X. C. *ACS Nano* **2011**, *5*, 7818.

(46) Zhai, H. J.; Pan, L. L.; Dai, B.; Kiran, B.; Li, J.; Wang, L. S. *J. Phys. Chem. C* **2008**, *112*, 11920.

(47) Hvolbæk, B.; Janssens, T. V. W.; Clausen, B. S.; Falsig, H.; Christensen, C. H.; Nørskov, J. K. *Nano Today* **2007**, *2*, 14.

(48) Cossaro, A.; Mazzarello, R.; Rousseau, R.; Casalis, L.; Verdini, A.; Kohlmeyer, A.; Floreano, L.; Scandolo, S.; Morgante, A.; Klein, M. *Science* **2008**, *321*, 943.

(49) de Bas, B. S.; Ford, M.; Cortie, M. *J. Phys.: Condens. Matter* **2005**, *18*, 55.

(50) Krishnamurty, S.; Shafai, G. S.; Kanhere, D.; de Bas, B. S.; Ford, M. *J. Phys. Chem. A* **2007**, *111*, 10769.

(51) Mazzarello, R.; Cossaro, A.; Verdini, A.; Rousseau, R.; Casalis, L.; Danisman, M. F.; Floreano, L.; Scandolo, S.; Morgante, A.; Scoles, G. *Phys. Rev. Lett.* **2007**, *98*, No. 016102.
(52) Farnesi Camellone, M.; Marx, D. *J. Phys. Chem. Lett.* **2013**, *4*, 514.
(53) Haruta, M.; Kobayashi, T.; Sano, H.; Yamada, N. *Chem. Lett.* **1987**, *16*, 405.
(54) Haruta, M. *Catal. Today* **1997**, *36*, 153.
(55) Haruta, M.; Daté, M. *Appl. Catal. A* **2001**, *222*, 427.
(56) Date, M.; Haruta, M. *J. Catal.* **2001**, *201*, 221.
(57) Hutchings, G. J. *Gold Bull.* **1996**, *29*, 123.
(58) Hutchings, G. J. *Catal. Today* **2002**, *72*, 11.
(59) Chen, M.; Cai, Y.; Yan, Z.; Goodman, D. W. *J. Am. Chem. Soc.* **2006**, *128*, 6341.
(60) Wörz, A. S.; Heiz, U.; Cinquini, F.; Pacchioni, G. *J. Phys. Chem. B* **2005**, *109*, 18418.
(61) Haruta, M. *Gold Bull.* **2004**, *37*, 27.
(62) Madsen, G. K. H.; Hammer, B. *J. Chem. Phys.* **2009**, *130*, No. 044704.
(63) Remediakis, I. N.; Lopez, N.; Nørskov, J. K. *Angew. Chem., Int. Ed.* **2005**, *117*, 1858.
(64) Fu, Q.; Saltsburg, H.; Flytzani-Stephanopoulos, M. *Science* **2003**, *301*, 935.
(65) Fu, L.; Wu, N.; Yang, J.; Qu, F.; Johnson, D.; Kung, M.; Kung, H.; Dravid, V. *J. Phys. Chem. B* **2005**, *109*, 3704.
(66) Liu, Z. P.; Jenkins, S. J.; King, D. A. *Phys. Rev. Lett.* **2005**, *94*, No. 196102.
(67) Bond, G.; Thompson, D. *Gold Bull.* **2000**, *33*, 41.
(68) Wang, J.; Hammer, B. *Top. Catal.* **2007**, *44*, 49.
(69) Zhang, C.; Michaelides, A.; King, D. A.; Jenkins, S. J. *J. Am. Chem. Soc.* **2010**, *132*, 2175.
(70) Wang, J.; Hammer, B. *Phys. Rev. Lett.* **2006**, *97*, No. 136107.
(71) Okazaki, K.; Morikawa, Y.; Tanaka, S.; Tanaka, K.; Kohyama, M. *Phys. Rev. B* **2004**, *69*, No. 235404.
(72) Ricci, D.; Bongiorno, A.; Pacchioni, G.; Landman, U. *Phys. Rev. Lett.* **2006**, *97*, No. 036106.
(73) Yoon, B.; Häkkinen, H.; Landman, U.; Wörz, A. S.; Antonietti, J.-M.; Abbet, S.; Judai, K.; Heiz, U. *Science* **2005**, *307*, 403.
(74) Harding, C.; Habibpour, V.; Kunz, S.; Farnbacher, A. N. S.; Heiz, U.; Yoon, B.; Landman, U. *J. Am. Chem. Soc.* **2009**, *131*, 538.
(75) Schubert, M. M.; Hackenberg, S.; van Veen, A. C.; Muhler, M.; Plzak, V.; Behm, R. J. *J. Catal.* **2001**, *197*, 113.
(76) Grisel, R.; Nieuwenhuys, B. *J. Catal.* **2001**, *199*, 48.
(77) Grisel, R.; Weststrate, K. J.; Gluhoi, A.; Nieuwenhuys, B. E. *Gold Bull.* **2002**, *35*, 39.
(78) Liu, X.; Wang, A.; Yang, X.; Zhang, T.; Mou, C. Y.; Su, D. S.; Li, J. *Chem. Mater.* **2008**, *21*, 410.
(79) Häkkinen, H.; Landman, U. *J. Am. Chem. Soc.* **2001**, *123*, 9704.
(80) Lopez, N.; Nørskov, J. K. *J. Am. Chem. Soc.* **2002**, *124*, 11262.
(81) Lang, S. M.; Bernhardt, T. M.; Barnett, R. N.; Yoon, B.; Landman, U. *J. Am. Chem. Soc.* **2009**, *131*, 8939.
(82) Xu, Y.; Mavrikakis, M. *J. Phys. Chem. B* **2003**, *107*, 9298.
(83) Widmann, D.; Behm, R. J. *Angew. Chem., Int. Ed.* **2011**, *50*, 10241.
(84) Kim, H. Y.; Lee, H. M.; Henkelman, G. *J. Am. Chem. Soc.* **2012**, *134*, 1560.
(85) Molina, L.; Rasmussen, M.; Hammer, B. *J. Chem. Phys.* **2004**, *120*, 7673.
(86) Molina, L.; Hammer, B. *Appl. Catal. A* **2005**, *291*, 21.
(87) Carrettin, S.; Hao, Y.; Aguilar-Guerrero, V.; Gates, B. C.; Trasobares, S.; Calvino, J. J.; Corma, A. *Chem—Eur. J.* **2007**, *13*, 7771.
(88) Chen, M.; Goodman, D. *Top. Catal.* **2007**, *44*, 41.
(89) Chrétien, S.; Metiu, H. *J. Chem. Phys.* **2007**, *127*, No. 084704.
(90) Chrétien, S.; Metiu, H. *J. Chem. Phys.* **2007**, *127*, No. 244708.
(91) Chrétien, S.; Metiu, H. *J. Chem. Phys.* **2007**, *126*, No. 104701.
(92) Wahlström, E.; Lopez, N.; Schaub, R.; Thostrup, P.; Rønnau, A.; Africh, C.; Lægsgaard, E.; Nørskov, J. K.; Besenbacher, F. *Phys. Rev. Lett.* **2003**, *90*, No. 026101.
(93) Fierro-Gonzalez, J. C.; Guzman, J.; Gates, B. C. *Top. Catal.* **2007**, *44*, 103.
(94) Hutchings, G. J.; Hall, M. S.; Carley, A. F.; Landon, P.; Solsona, B. E.; Kiely, C. J.; Herzing, A.; Makkee, M.; Moulijn, J. A.; Overweg, A. *J. Catal.* **2006**, *242*, 71.
(95) Weiher, N.; Beesley, A. M.; Tsapatsaris, N.; Delannoy, L.; Louis, C.; van Bokhoven, J. A.; Schroeder, S. L. M. *J. Am. Chem. Soc.* **2007**, *129*, 2240.
(96) Guzman, J.; Gates, B. C. *J. Am. Chem. Soc.* **2004**, *126*, 2672.
(97) Sanchez, A.; Abbet, S.; Heiz, U.; Schneider, W.-D.; Häkkinen, H.; Barnett, R.; Landman, U. *J. Phys. Chem. A* **1999**, *103*, 9573.
(98) Farnesi Camellone, M.; Zhao, J.; Jin, L.; Wang, Y.; Muhler, M.; Marx, D. *Angew. Chem., Int. Ed.* **2013**, *52*, 5780.
(99) Hong, S.; Rahman, T. S. *J. Am. Chem. Soc.* **2013**, *135*, 7629.
(100) Green, I. X.; Tang, W.; Neurock, M.; Yates, J. T. *Science* **2011**, *333*, 736.
(101) Liu, Z. P.; Gong, X. Q.; Kohanoff, J.; Sanchez, C.; Hu, P. *Phys. Rev. Lett.* **2003**, *91*, No. 266102.
(102) Liu, Z.-P.; Hu, P.; Alavi, A. *J. Am. Chem. Soc.* **2002**, *124*, 14770.
(103) http://www.cp2k.org/, 2010.
(104) VandeVondele, J.; Krack, M.; Mohamed, F.; Parrinello, M.; Chassaing, T.; Hutter, J. *Comput. Phys. Commun.* **2005**, *167*, 103.
(105) Perdew, J. P.; Burke, K.; Ernzerhof, M. *Phys. Rev. Lett.* **1996**, *77*, 3865.
(106) VandeVondele, J.; Hutter, J. *J. Chem. Phys.* **2007**, *127*, No. 114105.
(107) Lippert, B. G.; Hutter, J.; Parrinello, M. *Mol. Phys.* **1997**, *92*, 477.
(108) Goedecker, S.; Teter, M.; Hutter, J. *Phys. Rev. B* **1996**, *54*, 1703.
(109) Krack, M. *Theor. Chem. Acc.* **2005**, *114*, 145.
(110) Dudarev, S. L.; Botton, G. A.; Savrasov, S. Y.; Humphreys, C. J.; Sutton, A. P. *Phys. Rev. B* **1998**, *57*, 1505.
(111) Borodin, A.; Reichling, M. *Phys. Chem. Chem. Phys.* **2011**, *13*, 15442.
(112) Aiura, Y.; Nishihara, Y.; Haruyama, Y.; Komeda, T.; Kodaira, S.; Sakisaka, Y.; Maruyama, T.; Kato, H. *Phys. B (Amsterdam, Neth.)* **1994**, *194*, 1215.
(113) Zhang, Z.; Yoon, Y.; Lin, X.; Acharya, D.; Kay, B. D.; Rousseau, R.; Dohnálek, Z. *J. Phys. Chem. Lett.* **2012**, *3*, 3257.
(114) Molina, L. M.; Hammer, B. *J. Catal.* **2005**, *233*, 399.
(115) Nosé, S. *J. Chem. Phys.* **1984**, *81*, 511.
(116) Hoover, W. G. *Phys. Rev. A* **1985**, *31*, 1695.
(117) Mills, G.; Jónsson, H.; Schenter, G. K. *Surf. Sci.* **1995**, *324*, 305.
(118) Henkelman, G.; Uberuaga, B. P.; Jónsson, H. *J. Chem. Phys.* **2000**, *113*, 9901.
(119) Rousseau, R.; De Renzi, V.; Mazzarello, R.; Marchetto, D.; Biagi, R.; Scandolo, S.; del Pennino, U. *J. Phys. Chem. B* **2006**, *110*, 10862.
(120) Deskins, N. A.; Rousseau, R.; Dupuis, M. *J. Phys. Chem. C* **2009**, *113*, 14583.
(121) Heimel, G.; Romaner, L.; Brédas, J.-L.; Zojer, E. *Phys. Rev. Lett.* **2006**, *96*, No. 196806.
(122) Beck, T. L.; Doll, J.; Freeman, D. L. *J. Chem. Phys.* **1989**, *90*, 5651.
(123) Tong, X.; Benz, L.; Chrétien, S.; Metiu, H.; Bowers, M. T.; Buratto, S. K. *J. Phys. Chem. C* **2010**, *114*, 3987.
(124) Bond, G. C.; Thompson, D. T. *Catal. Rev.* **1999**, *41*, 319.
(125) Huizinga, T.; van 'T Blik, H. F. J.; Vis, J. C.; Prins, R. *Surf. Sci.* **1983**, *135*, 580.
(126) Liu, J. J. *ChemCatChem* **2011**, *3*, 934.
(127) Jiang, Z.; Zhang, W.; Jin, L.; Yang, X.; Xu, F.; Zhu, J.; Huang, W. *J. Phys. Chem. C* **2007**, *111*, 12434.
(128) Du, Y.; Deskins, N. A.; Zhang, Z.; Dohnalek, Z.; Dupuis, M.; Lyubinetsky, I. *Phys. Chem. Chem. Phys.* **2010**, *12*, 6337.
(129) Papageorgiou, A. C.; Beglitis, N. S.; Pang, C. L.; Teobaldi, G.; Cabailh, G.; Chen, Q.; Fisher, A. J.; Hofer, W. A.; Thornton, G. *Proc. Natl. Acad. Sci. U. S. A.* **2010**, *107*, 2391.
(130) Chrétien, S.; Metiu, H. *J. Chem. Phys.* **2008**, *128*, No. 044714.

(131) Finazzi, E.; Di Valentin, C.; Pacchioni, G. *J. Phys. Chem. C* **2009**, *113*, 3382.
(132) Deskins, N. A.; Dupuis, M. *J. Phys. Chem. C* **2008**, *113*, 346.
(133) Deskins, N. A.; Rousseau, R.; Dupuis, M. *J. Phys. Chem. C* **2010**, *114*, 5891.
(134) Liu, L.; McAllister, B.; Ye, H.; Hu, P. *J. Am. Chem. Soc.* **2006**, *128*, 4017.
(135) Yang, X. F.; Wang, Y. L.; Zhao, Y. F.; Wang, A. Q.; Zhang, T.; Li, J. *Phys. Chem. Chem. Phys.* **2010**, *12*, 3038.
(136) Pal, R.; Huang, W.; Wang, Y. L.; Hu, H. S.; Bulusu, S.; Xiong, X. G.; Li, J.; Wang, L. S.; Zeng, X. C. *J. Phys. Chem. Lett.* **2011**, *2*, 2288.
(137) Hrbek, J.; Hoffmann, F. M.; Park, J. B.; Liu, P.; Stacchiola, D.; Hoo, Y. S.; Ma, S.; Nambu, A.; Rodriguez, J. A.; White, M. G. *J. Am. Chem. Soc.* **2008**, *130*, 17272.
(138) Li, W.-K.; Chu, L.-N.; Gong, X.-Q.; Lu, G. *Surf. Sci.* **2011**, *605*, 1369.
(139) McKenna, K. P.; Shluger, A. L. *J. Phys. Chem. C* **2007**, *111*, 18848.
(140) Yang, J. H.; Henao, J. D.; Raphulu, M. C.; Wang, Y.; Caputo, T.; Groszek, A.; Kung, M. C.; Scurrell, M. S.; Miller, J. T.; Kung, H. H. *J. Phys. Chem. B* **2005**, *109*, 10319.
(141) Lin, S.; Bollinger, M.; Vannice, M. *Catal. Lett.* **1993**, *17*, 245.
(142) Starr, D. E.; Shaikhutdinov, S. K.; Freund, H.-J. *Top. Catal.* **2005**, *36*, 33.
(143) Yang, F.; Chen, M.; Goodman, D. *J. Phys. Chem. C* **2008**, *113*, 254.
(144) Ouyang, R.; Liu, J.; Li, W.-X. *J. Am. Chem. Soc.* **2012**, *135*, 1760.
(145) Negreiros, F. R.; Sementa, L.; Barcaro, G.; Vajda, S.; Aprá, E.; Fortunelli, A. *ACS Catal.* **2012**, *2*, 1860.
(146) Mavrikakis, M.; Stoltze, P.; Nørskov, J. K. *Catal. Lett.* **2000**, *64*, 101.
(147) Rodriguez, J. A. *Catal. Today* **2011**, *160*, 3.
(148) Park, J. B.; Graciani, J.; Evans, J.; Stacchiola, D.; Senanayake, S. D.; Barrio, L.; Liu, P.; Sanz, J. F.; Hrbek, J.; Rodriguez, J. A. *J. Am. Chem. Soc.* **2009**, *132*, 356.
(149) Rodríguez, J. A.; Evans, J.; Graciani, J.; Park, J. B.; Liu, P.; Hrbek, J.; Sanz, J. F. *J. Phys. Chem. C* **2009**, *113*, 7364.
(150) Stiehl, J. D.; Kim, T. S.; McClure, S. M.; Mullins, C. B. *J. Am. Chem. Soc.* **2004**, *126*, 13574.
(151) Molina, L.; Hammer, B. *Phys. Rev. B* **2004**, *69*, No. 155424.
(152) Remediakis, I. N.; Lopez, N.; Nørskov, J. K. *Appl. Catal. A* **2005**, *291*, 13.
(153) Green, I. X.; Tang, W.; McEntee, M.; Neurock, M.; Yates, J. T. *J. Am. Chem. Soc.* **2012**, *134*, 12717.
(154) Metiu, H.; Chrétien, S.; Hu, Z.; Li, B.; Sun, X. *J. Phys. Chem. C* **2012**, *116*, 10439.